Static Electromagnetic Field Computation by Conformal Mapping in Permanent Magnet Synchronous Machines

Martin Hafner, David Franck, and Kay Hameyer

Institute of Electrical Machines, RWTH Aachen University, Schinkelstraße 4, D-52062 Aachen, Germany

In modern servo drives or electrical drives for positioning, torque pulsation, tangential forces and ripple torque are undesirable effects. These parasitic effects are due to the presence of higher time and space harmonics in the air gap flux density. This paper presents a time-effective method to compute the radial and tangential field components under load and no-load condition by conformal mapping in the frequency domain. The proposed method is applied to a surface mounted permanent magnet synchronous machine, and compared to numeric results obtained by nonlinear FEA. The analytical results obtained by the conformal mapping are shown to be in good agreement to the finite element simulations.

Index Terms—**Air gap permeance, magnetic fields, permanent magnet motor, torque.**

I. Introduction

THE design of electrical machines is routinely done by means of virtual prototyping nowadays in order to reduce costs and shorten the time-to-market. Besides FEA, which is computationally expensive, analytical models are also used to obtain a quick first approximation of the machine's behavior. Conventional analytical models usually focus on the determination of the fundamental air gap flux density. Consequently, the effect of air gap field harmonics on the main machine characteristics, like EMF, cogging-torque and load-torque, as well as the impact of geometry variations on those quantities are neglected. In this paper, an analytic conformal mapping method in frequency domain for permanent magnet synchronous machines (PMSM) is applied. This alternative method considers the occurring air gap field harmonics for torque and EMF computation. Although this method assumes the magnetic permeability of all magnetic materials in infinite, the comparison with standard nonlinear FEA shows that it nevertheless gives a good approximation of the air gap flux density spectrum and all derived quantities.

II. Computational Framework

A. Rotor Field Distribution in the Slotless Stator

The analytical technique for computing the 2D magnetic field distribution in the air gap of radial-magnetized permanent magnet rotors at no-load has been described in [1]. The derived parametric field solution is applicable for both internal and external rotors. In further researches, the approach has been generalized to radial and parallel magnetizations, [2]. Recently, [3] published a further extension to radial sine and sinusoidal direction magnetizations. In case of a slotless stator, the radial flux density $B_r(\Theta)$ and the tangential flux density $B_\varphi(\Theta)$ can be expressed in terms of a Fourier Series

$$B_r(\Theta) + \jmath B_\varphi(\Theta) = \sum_{n=0}^{\infty} (B_{r,n} + \jmath B_{\varphi,n}) e^{\jmath p \Theta} \qquad (1)$$

where n is the frequency order, p the number of pole pairs, Θ the mechanical angle. In this representation of the air gap field, the Fourier coefficients $B_{r,n}$ and $B_{\varphi,n}$ are the solution of a linear Laplace problem with magnets and a slotless stator.

B. Rotor Field Distribution in the Slotted Stator

Stator slotting significantly influences the magnetic field distribution as follows:

1) The different radial magnetic permeances of teeth and slots affect the local distribution of the flux in the air gap. A flux concentration beneath the teeth can be observed;
2) A peak of the flux density is also observed at the PM vertices in the air gap;
3) Slotting mixes up radial and tangential components.

A standard method for modeling these effects is known as "permeance functions" in literature. In that of [4], only the impact of effect 1) on the radial flux density component is computed. The recent publications [5], [6] derive by four complex conformal mappings, including a Schwarz-Christoffel transformation, a permeance function which takes the effects 1)–3) into account. Assuming a magnetic core with infinite permeability, this ansatz has shown to yield identical flux density results in comparison to FE simulation applying Neumann boundary conditions.

For that approach, the conformal transformations are used to transform slotted stator geometry into a slottless stator, for which the Laplace equation governing the air gap field can be solved analytically. By this, the impact of slotting on the field distribution keeps considered. Correlating the field distribution with slotting, ${}^{s}B$, to the field without slotting (1) yields the complex permeance $\underline{\lambda}$

$${}^{s}\underline{B}(\Theta) = (B_r + \jmath B_\varphi)\underline{\lambda}^{*} \qquad (2)$$

which describes the individual characteristic of the slotting on the field.

Even if the Laplace equation can be solved analytically, the combined governing equations can not be solved directly. Therefore the position-dependent complex permeance $\underline{\lambda}$ is evaluated numerically by means of a nonlinear iterative solution. At each point of an equidistant sampled arc in the air gap with

Manuscript received December 14, 2009; accepted February 13, 2010. Current version published July 21, 2010. Corresponding author: M. Hafner (e-mail: Martin.Hafner@IEM.RWTH-Aachen.de).

Color versions of one or more of the figures in this paper are available online at http://ieeexplore.ieee.org.

Digital Object Identifier 10.1109/TMAG.2010.2043930

0018-9464/$26.00 © 2010 IEEE

the length of one slot pitch, the complex permeance number, that fulfills (2), writes

$$\underline{\lambda} = \lambda_r + \jmath\lambda_\varphi \tag{3}$$

where λ_r and λ_φ represent the permeance variations in radial and tangential direction. The sampled permeance can be expressed by a Fourier-Series and extended to the whole air gap, yielding

$$\underline{\lambda}(\Theta) = \sum_{0}^{N_\lambda} \lambda_{r,n}\cos(nN_s\Theta) + \jmath\sum_{1}^{N_\lambda} \lambda_{\varphi,n}\sin(nN_s\Theta) \tag{4}$$

where N_s is the number of stator teeth and N_λ the sampling rate, depending on the largest frequency occurring in the system.

C. Armature Winding Field

The magnetic field distribution due to a current in a single slot, assuming a infinite slot depth and a infinite permeability in a slotless stator, can be obtained by three successive conformal mappings [7]. Since coils occupy two slots with opposite directed currents, a flux density distribution ${}^c\underline{B}$ for the whole air gap per coil can be assembled in functions of the coil current I_c and the number coil turns N as

$${}^c\underline{B}(\Theta, N, I_c) = NI_c\sum_{1}^{N_a}\left({}^cB_{r,n} + \jmath{}^cB_{\varphi,n}\right)e^{\jmath n\Theta} \tag{5}$$

where N_a denotes the maximal frequency order and the radial and tangential quantities ${}^cB_{r,n}$ and ${}^cB_{\varphi,n}$ the Fourier coefficients of the coil computed for one ampere. According to the winding schema of the PMSM a flux distribution ${}^pB$ for all phases can be found by adding shifted copies of (5). In case of a symmetric current load (UVW) I, the allover armature field ${}^a\underline{B}$ is given by

$${}^aB(\Theta, I) = ({}^p\underline{B}_U, {}^p\underline{B}_V, {}^p\underline{B}_W) \times \left(e^{\jmath\phi_q}, e^{\jmath(\phi_q+120^\circ)}, e^{\jmath(\phi_q+240^\circ)}\right)^T \tag{6}$$

where the angle ϕ_q defines the relative phase orientation to the quadrature axis of the machine.

D. Field Distribution in the Slotted Air Gap

The magnetic air gap field in case of stator slotting can be assumed to be the superposition of the field component fields due to the permanent magnets and all stator currents.

Introducing a time-discretization Δ_{FE}

$$\Delta_{\mathrm{FE}} = \frac{1}{n\cdot N_{el}\cdot p} \tag{7}$$

where n is the mechanical rotor speed and N_{el} the number of computation steps per electric period, a certain instance of time t can be addressed with the step index n_{FE} as

$$t = \Delta_{\mathrm{FE}} n_{\mathrm{FE}}. \tag{8}$$

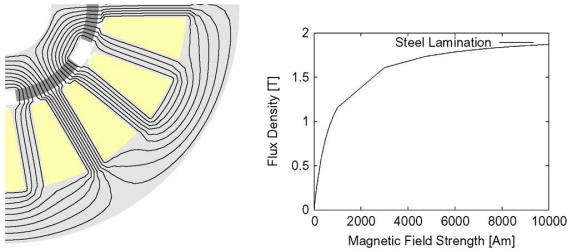

(a) (b)

Fig. 1. Application Data. (a) Cross section of PMSM. (b) BH characteristic of steel lamination.

Adding rotor movement in the sense of (8) to (2), the rotor flux distribution is

$${}^s\underline{B}^t(f) = {}^s\underline{B}(\Theta)e^{\jmath 2\pi t}. \tag{9}$$

The argument of the function ${}^s\underline{B}^t$ denotes a notation in frequency domain. The corresponding time-depend armature field is frequency-shifted by the stator frequency f_1, yielding

$${}^a\underline{B}^t(f, I) = {}^a\underline{B}(\Theta, I)e^{\jmath 2\pi f_1 t}. \tag{10}$$

The frequency shifting in (9) and (10) by the rotor frequency, not the rotor position, is optional and is given here for the sake of completeness.

E. Torque Computation by Maxwell Stress Theory

The theory of electromagnetic forces states, that the resulting force on a rigid compound placed in a magnetic field is given by the integral of the magnetic stress tensor over the closed body surface. For PM motors, the stress is evaluated on a cylindrical surface placed in the middle of the machine's air gap. For torque computation, only the tangential stress component is of significance, so that the integral form of the torque is

$$T = \frac{lr^2}{\mu_0}\int_0^{2\pi} B_r(\Theta)B_\varphi(\Theta)d\Theta \tag{11}$$

where l is the stack length, r the radius of the cylindrical surface and B_r, B_φ the position dependent radial and tangential air gap flux densities on the cylinder. Substituting (9), (10) yields

$$T(t) = \frac{l_z(r_{orr}+h_\delta)^2}{\mu_0}\left[\left({}^sB_r^t + {}^aB_r^t\right) * \left({}^sB_\varphi^t + {}^aB_\varphi^t\right)\right]_{DC} \tag{12}$$

where DC denotes the constant component of the convolution. A detailed discussion of different methodologies for analytic torque computation can be found in [8], [9].

III. Application

To demonstrate the proposed method, a PMSM is investigated with a nonlinear two dimensional transient FE solver, and with the conformal mapping (CM) approach. The cross-section of the motor is pictured in Fig. 1(a), all parameters of the dimension and the electromagnetic evaluation are in listed in Table I. Both methods (FEA, CM) are carried out with 60 steps per period (N_{el}), which leads to a time step of $t = 10^{-4}$ s. The nonlinearity of the laminated steel characteristic is taken into account in case of FEA by the BH curve sketched in Fig. 1(b).

TABLE I
PARAMETERS FOR SIZING AND ELECTROMAGNETIC EVALUATION

p	3	Number of Pole Pairs
N_s	18	Number of Stator Teeth
P_r	1520 W	Rated Power
n_r	3000 rpm	Rated Speed
τp	0.73	Pole Pitch Factor
h_m	3 mm	Permanent Magnet Height
r_{orr}	24.5 mm	Outer Rotor Radius (inc. PM)
h_δ	0.8 mm	Air Gap Height
h_{stth}	0.5 mm	Stator Tooth Tip Height
h_{sth}	21.7 mm	Stator Tooth Height
r_{osr}	54.2 mm	Outer Stator Radius
h_{stw}	5 mm	Stator Tooth Width
h_{sow}	1.5 mm	Slot Opening Width
l_z	101 mm	Length
B_r	1.244 T	Remanence Flux Density
k_{cu}	30%	Copper Fill Factor

A. No Load Simulation

Conformal mapping technique implies an infinite steel permeability. Therefore, only the slot opening width i.e. the distance, measured between tooth tips, contributes to the field characteristic. To analyze the impact of tooth tip saturation, which occurs even in no load operation, the comparison of CM and FEA is carried out for the dimensions of Table I and two variations, where the slots are almost opened ($h_{sow} = 2.5\ \mathrm{mm}$) and closed ($h_{sow} = 0.5\ \mathrm{mm}$). Fig. 2 shows the comparison of the radial and tangential flux density distribution in the air gap over a pole pitch, by FEA and CM. Since first order finite elements have a constant flux density, numerical noise appears in the distribution calculated by the FEA. In all cases, FEA and CM graphs have the same shape and are located closely to each other. The effect of tip saturation on the radial component B_r increases by decreasing the slot opening width and leads to maximal relative error of about 2% ($h_{sow} = 2.5\ \mathrm{mm}$). This also side effects the tangential component B_φ, where local deviations between both curves can be found beside the slot openings at 110° and 130°.

The back EMF is derived from the no load phase flux linkage Φ_{U-X} of PM motors according the Faraday's law

$$U^{emf}_{U-X}(t) = -\frac{d\Phi_{U-X}}{dt}. \tag{13}$$

In case of CM the flux linkage is equal to the integral of the radial air gap flux density over a coil pitch, defined by the positions U_1 and X_1, yielding

$$\Phi_{U-X}(t) = l_z(r_{orr} + h_\delta)w \int_{U_1}^{X_1} {}^s B_r^t(\Theta) d\Theta \tag{14}$$

where w are the number of turns per phase. Fig. 3(a) compares the flux obtained by FEA and CM in function of the rotor position for the original drive. An overview of the absolute error within each time step for all design variation is sketched in Fig. 3(b), showing low deviations in all cases.

The cogging torque is very sensitive to the slot opening and the steel properties. The torque computation by (12) is carried out for all variation in Fig. 4. Due to the symmetry of the machine, given in Table I, the torque results are presented over an electrical angle of 60°. For Fig. 4(a) and (c), the curves progressions are located closely to each other, whereas b) shows that CM does not cover the attenuated damping effects of nearly closed slots and therefore overestimates the occurring forces.

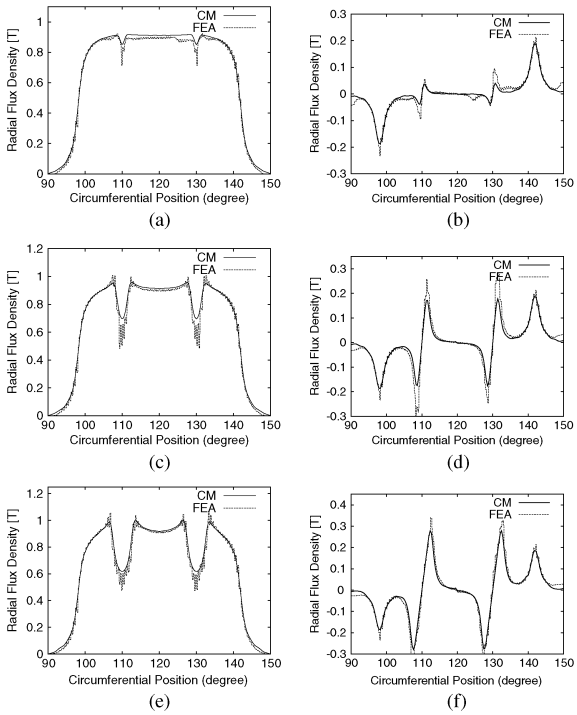

Fig. 2. Comparison of radial and tangential flux density distribution in the air gap over PMSM pole pitch by FEA and conf. mapping (CM) in no load operation for different slot opening width. (a) B_r for $h_{sow} = 0.5\ \mathrm{mm}$. (b) B_φ for $h_{sow} = 0.5\ \mathrm{mm}$. (c) B_r for $h_{sow} = 1.5\ \mathrm{mm}$. (d) B_φ for $h_{sow} = 1.5\ \mathrm{mm}$. (e) B_r for $h_{sow} = 2.5\ \mathrm{mm}$. (f) B_φ for $h_{sow} = 2.5\ \mathrm{mm}$.

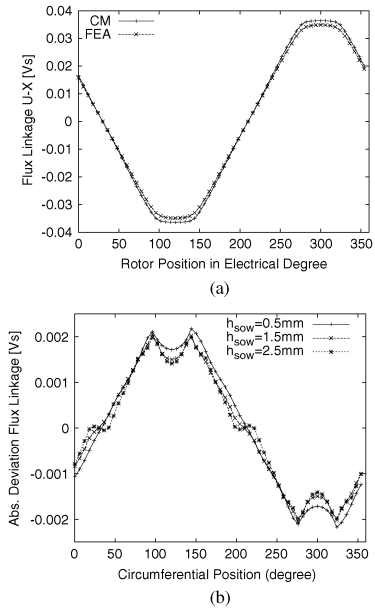

Fig. 3. Comparison of phase flux linkage obtained by FEA and CM in no load operation. (a) Flux linkage for machine design with $h_{sow} = 1.5\ \mathrm{mm}$. (b) Absolute deviation of flux linkage for all design candidates.

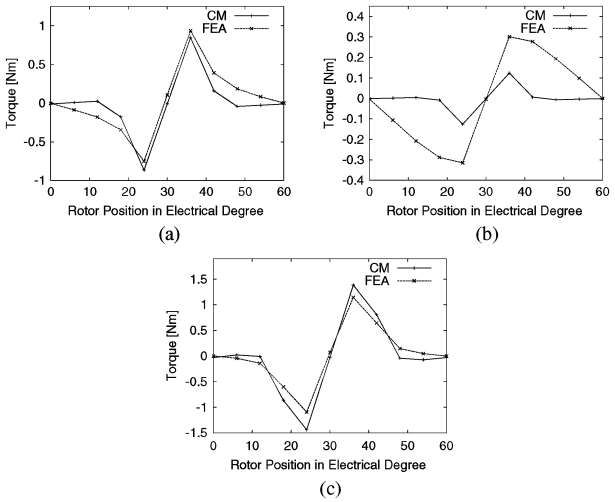

Fig. 4. Comparison of cogging torque obtained by FEA and CM. (a) Torque for machine design with $h_{sow} = 1.5$ mm. (b) Torque for machine design with $h_{sow} = 0.5$ mm. (c) Torque for machine design with $h_{sow} = 2.5$ mm.

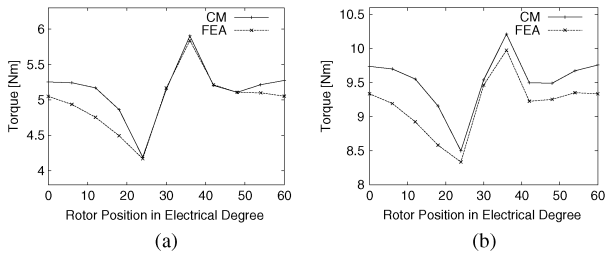

Fig. 5. Comparison of load and overload torque obtained by FEA and CM (Time Domain). (a) Torque for $J = 6(\mathrm{A/mm^2})$. (b) Torque for $J = 11(\mathrm{A/mm^2})$.

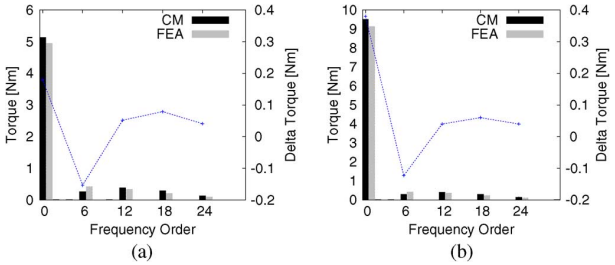

Fig. 6. Comparison of load and overload torque obtained by FEA and CM (frequency domain). (a) Torque for $J = 6(\mathrm{A/mm^2})$. (b) Torque for $J = 11(\mathrm{A/mm^2})$.

B. Load Simulation

The presented approach is also capable of computing the air gap flux density distribution under arbitrary, even unsymmetrical, load situation, compare (5). The load simulation is performed for a rated current density of about 6 $\mathrm{A/mm^2}$ and an overload operation of 11 $\mathrm{A/mm^2}$. In both cases the current phasor is aligned with the quadrature axis. The torque diagrams in function of the rotor angle are given in Fig. 5. It can be seen that the torque obtained analytically is close to the results of FEA for $J = 6(\mathrm{A/mm^2})$. For $J = 11(\mathrm{A/mm^2})$, the shape of the curves are similar but the magnitude do not match. A comparison of the occurring torque harmonics for both load situations is given in Fig. 6. The scale on the right hand side shows the absolute torque deviation between the values for each frequency order. For rated operation the harmonics of CM are well matching with those of FEA, with a difference in the constant torque component of 0.2 Nm.

C. Computational Effort

The conformal ansatz functions for rotor and stator flux density are machine characteristics, which depend only on its dimension and can be computed within a few seconds. Once computed, each feasible operation point is evaluated by a convolution in frequency domain, compare (12) and (14). Even if a transient 2D FEA of an operation point lasts a few minutes, the presented approach has nearly real time capabilities.

IV. Conclusion

Electromagnetic field computations are ubiquitous in electrical machine design. Even if the finite-element method yields very accurate results, its high computational effort inhibits an application in early design stages or multi-object optimizations of electrical drives. In that case, it is worth seeking for approximative and time-saving alternatives. In this paper, the air gap field of a PMSM under load and no-load has been computed by conformal mapping in frequency domain in order to evaluate flux linkage, EMF and torque. The results are compared to data obtained by nonlinear 2D FEA, to validate the proposed method and to identify inherent weaknesses, which follow from the misrepresentation of the magnetic permeability of iron cores. For the considered application examples, the analyzed quantities are in good agreement with FEA. A variation of the tooth's width shows a significant overestimation of the cogging torque for nearly closed slots. The knowledge of the air gap flux density distributions is the starting point for electromagnetic structure dynamic or acoustic computation. In the present state, the conformal mapping does not consider a saturation term, which prevents an application to drives in deep saturation. Further investigations are necessary to clarify the impact on the torque and flux computation.

References

[1] Z. Zhu and D. Howe, "Instantaneous magnetic field distribution in brushless permanent magnet DC motors—III: Effect of stator slotting," *IEEE Trans. Magn.*, vol. 29, no. 1, pp. 143–151, 1993.

[2] Z. Zhu, D. Howe, and C. Chan, "Improved analytical model for predicting the magnetic field distribution in brushless permanent-magnet machines," *IEEE Trans. Magn.*, vol. 38, no. 1, pp. 229–238, 2002.

[3] D. C. Hanselman, *Brushless Permanent Magnet Motor Design*, 2nd ed. Cranston, RI: The Writers' Collective, Mar. 2003.

[4] Z. Zhu, D. Howe, E. Bolte, and B. Ackermann, "Instantaneous magnetic field distribution in brushless permanent magnet DC motors—I: Open-circuit field," *IEEE Trans. Magn.*, vol. 29, no. 1, pp. 124–135, 1993.

[5] D. Zarko, D. Ban, and T. Lipo, "Analytical calculation of magnetic field distribution in the slotted air gap of a surface permanent-magnet motor using complex relative air-gap permeance," *IEEE Trans. Magn.*, vol. 42, no. 7, pp. 1828–1837, 2006.

[6] D. Zarko, D. Ban, and T. Lipo, "Analytical solution for cogging torque in surface permanent-magnet motors using conformal mapping," *IEEE Trans. Magn.*, vol. 44, no. 1, pp. 52–65, 2008.

[7] K. J. Binns, *Analysis and Computation of Electric and Magnetic Field Problems*. New York: Pergamon Press, 1963, [distributed in the Western Hemisphere by Macmillan, New York].

[8] E. Starschich, A. Muetze, and K. Hameyer, "Analytical force calculation in brushless-DC motors i: An alternative approach," in *Proc. IEEE Int. Electric Machines and Drives Conf.*, 2009, pp. 1200–1207.

[9] E. Starschich, A. Muetze, and K. Hameyer, "Analytical force calculation in brushless-dc motors II: Mathematical details of the alternative approach," in *Proc. IEEE Int. Electric Machines and Drives Conf.*, 2009, pp. 1208–1215.